AGU PUBLICATIONS

JGR

Journal of Geophysical Research: Oceans

RESEARCH ARTICLE

10.1002/2016JC011714

Mesoscale modulation of air-sea CO_2 flux in Drake Passage

Hajoon Song[1], John Marshall[1], David R. Munro[2], Stephanie Dutkiewicz[1], Colm Sweeney[3,4], D. J. McGillicuddy Jr.[5], and Ute Hausmann[5]

[1]Department of Earth, Atmospheric and Planetary Sciences, Massachusetts Institute of Technology, Cambridge, Massachusetts, USA, [2]Department of Atmospheric and Oceanic Sciences and Institute of Arctic and Alpine Research, University of Colorado, Boulder, Colorado, USA, [3]Cooperative Institute for Research in Environmental Sciences, University of Colorado, Boulder, Colorado, USA, [4]NOAA Earth System Research Laboratory, Boulder, Colorado, USA, [5]Department of Applied Ocean Physics and Engineering, Woods Hole Oceanographic Institution, Woods Hole, Massachusetts, USA

Key Points:
- Both observations and models reveal mesoscale modulation of CO_2 flux near Drake Passage
- CO_2 flux varies seasonally due to the changes in the balance between solubility and biogeochemical effects
- Anomalous vertical mixing is the key physical process that drives CO_2 flux modulation

Correspondence to:
H. Song,
hajsong@mit.edu

Citation:
Song, H., J. Marshall, D. R. Munro, S. Dutkiewicz, C. Sweeney, D. J. McGillicuddy, and U. Hausmann (2016), Mesoscale modulation of air-sea CO_2 flux in Drake Passage, *J. Geophys. Res. Oceans*, *121*, 6635–6649, doi:10.1002/2016JC011714.

Received 9 FEB 2016
Accepted 20 JUN 2016
Accepted article online 24 AUG 2016
Published online 10 SEP 2016

Abstract We investigate the role of mesoscale eddies in modulating air-sea CO_2 flux and associated biogeochemical fields in Drake Passage using in situ observations and an eddy-resolving numerical model. Both observations and model show a negative correlation between temperature and partial pressure of CO_2 (pCO_2) anomalies at the sea surface in austral summer, indicating that warm/cold anticyclonic/cyclonic eddies take up more/less CO_2. In austral winter, in contrast, relationships are reversed: warm/cold anticyclonic/cyclonic eddies are characterized by a positive/negative pCO_2 anomaly and more/less CO_2 outgassing. It is argued that DIC-driven effects on pCO_2 are greater than temperature effects in austral summer, leading to a negative correlation. In austral winter, however, the reverse is true. An eddy-centric analysis of the model solution reveals that nitrate and iron respond differently to the same vertical mixing: vertical mixing has a greater impact on iron because its normalized vertical gradient at the base of the surface mixed layer is an order of magnitude greater than that of nitrate.

1. Introduction

The Southern Ocean (SO) is the largest sink of anthropogenic carbon dioxide (CO_2), taking up roughly one third of the global inventory [*Mikaloff Fletcher et al.*, 2006; *Gruber et al.*, 2009; *Lenton et al.*, 2013]. At the same time, the SO releases natural CO_2 into the atmosphere, partially canceling out anthropogenic uptake [*Gruber et al.*, 2009]. Several modeling and observational studies suggest that the SO may have become less effective in taking up anthropogenic CO_2 over the last several decades [*Metzl*, 2009; *Le Quéré et al.*, 2010; *Lovenduski et al.*, 2013]. A large-scale analysis by *Landschützer et al.* [2015] and regional studies by *Xue et al.* [2015] and *Munro et al.* [2015a], indicate that SO CO_2 uptake may have increased over the past decade. *Landschützer et al.* [2015] suggest that this recent increase in SO CO_2 uptake follows a decade in which CO_2 uptake stagnated consistent with previous studies, while an analysis by *Majkut et al.* [2014] suggest that no decrease in the effectiveness of SO CO_2 uptake has occurred.

The air-sea CO_2 flux in the SO has marked seasonal variability [*Takahashi et al.*, 2002; *Lenton et al.*, 2006; *Metzl et al.*, 2006; *Brix et al.*, 2013; *Lenton et al.*, 2013]. In austral summer, the ocean takes up CO_2 due to increased biological productivity. In austral winter, however, suppression of biological productivity and the upwelling of waters rich in dissolved inorganic carbon (DIC) increases surface ocean pCO_2. Over the last decade *Landschützer et al.* [2014] and *Munro et al.* [2015a] suggest that the sign of winter air-sea exchange may be into the ocean due to slower oceanic pCO_2 increase than that in the atmosphere. Surface pCO_2 is also sensitive to temperature through solubility effects and decreases/increases as temperature cools/warms. These two opposing effects (biogeochemistry and solubility) compensate one another reducing seasonal pCO_2 variability [*Jiang et al.*, 2014; *Munro et al.*, 2015b] relative to other parts of the ocean where these effects are not as well balanced [*Takahashi et al.*, 2002]. Even in the presence of compensation, observations show a seasonal variability in oceanic pCO_2 which is larger than that of atmospheric pCO_2 in both the Indian and west Pacific sectors [*Metzl et al.*, 2006; *Brix et al.*, 2013]. This indicates that the ocean plays an active role in air-sea CO_2 flux in the SO by changing the difference between oceanic and atmospheric pCO_2.

Mesoscale eddies, often identified by anomalies in sea surface height (SSH), modulate oceanic physical fields such as temperature, salinity, heat flux, heat content and vertical mixing [*Hausmann and Czaja*, 2012;

Stephenson et al., 2013; *Song et al*., 2015]. Cyclones typically have colder core temperatures than the surrounding fluid, resulting in anomalous heat uptake [e.g., *Williams*, 1988]. They are characterized by stronger stratification in the near surface ocean, since isopycnals dome upward, leading to shallower mixed layers. In the southern hemisphere, cyclones rotate clockwise and are associated with a negative SSH anomaly. In contrast, warm anticyclones are less stable with anomalous heat loss to the atmosphere, downward doming of isopycnals, weaker stratification and deeper mixed layers. Anticyclones rotate counter-clockwise with a positive SSH anomaly.

Mesoscale eddies can also impact biogeochemical fields such as nutrients and plankton in complex ways (i.e., stirring, trapping and isopycnal displacement, Ekman pumping from eddy-wind interaction, and anomalous vertical mixing, see *Gaube et al*. [2013]). In particular, the trapping mechanism can transport water parcels horizontally to other areas with different biogeochemical properties, and is more effective when there is a stronger lateral gradient. Isopycnal displacement changes the depth of the nutricline and affects the nutrient supply to the euphotic zone. Anticyclones/cyclones deepen/shoal isopycnals and the nutricline, resulting in less/more available nutrients. However deeper/shallower mixed layers in anticyclones/cyclones can provide more/less nutrients to the surface [*Kunze*, 1985; *Kunze et al*., 1995; *Koszalka et al*., 2010; *Song et al*., 2015; *Dufois et al*., 2016].

These complex impacts of mesoscale eddies in the SO have been reported in the literature. *Kahru et al*. [2007] observed that cyclones have enhanced chlorophyll biomass while anticyclones are marked with lower chlorophyll biomass in the Scotia Sea of the southwest Atlantic. However, *Meredith et al*. [2003] found an increased chlorophyll biomass in an anticyclonic eddy found above the northwest Georgia Rise in the Scotia Sea. *Korb and Whitehouse* [2004] argue that this is because of anomalously high iron supply from shelf sediments. *Thomalla et al*. [2011] report a complex interplay between mixed-layer depth and chlorophyll in the SO, which suggests that anomalies in vertical mixing associated with mesoscale eddies can have different impacts on the surface chlorophyll biomass depending on the region. Indeed, satellite observations of SSH and chlorophyll reveal complex relationships between mesoscale eddies and chlorophyll biomass in the SO, with both positive and negative cross correlations [*Gaube et al*., 2014].

Mesoscale eddies modulate air-sea CO_2 flux through anomalous physical and biogeochemical properties; however, it is not straightforward to anticipate how mesoscale eddies change CO_2 flux because the overall sign and magnitude are dependent on a complicated balance of physical and biological processes with sometimes opposing effects. In the high-nutrient low-chlorophyll SO, primary production is generally regulated by iron (Fe) [*Cooper et al*., 1996; *Boyd et al*., 2000; *Watson et al*., 2000] and light. Thus higher levels of biologically available Fe will result in enhanced primary production, leading to lower DIC, pCO_2 and either increased uptake or reduced outgassing of CO_2. Anticyclones may have less Fe if the downward displacement of isopycnals pushes Fe-rich water to a deeper level, leading to less primary production and CO_2 uptake. In contrast, anticyclones potentially lead to more CO_2 uptake if they trap Fe-rich water near the sediment sources and are transported offshore [*Korb and Whitehouse*, 2004]. If vertical mixing in the open ocean is deep enough to entrain Fe-rich subsurface water in anticyclones, we can also expect more CO_2 drawdown by enhanced primary production. Even in the presence of elevated Fe, the biological effect may be muted if anomalously deep mixed layers lead to light limitation, complicating the role of mesoscale eddies in modulating air-sea CO_2 flux.

In this study, we attempt to gain a deeper understanding of the role of cyclonic and anticyclonic eddies in modulating CO_2 flux in the region of Drake Passage over the seasonal cycle using repeat shipboard transects and an eddy-resolving ocean model. Both observations and model reveal mesoscale modulation of the CO_2 flux which varies seasonally. This is studied by separating the oceanic pCO_2 into temperature-driven and DIC-driven components. An eddy-centric analysis of the model simulation reveals a differing response of iron and nitrate to the same vertical mixing, which we link to the size of the vertical gradients at the base of the mixed layer.

Our paper is organized as follows. In section 2, we describe the observations of pCO_2 across the Drake Passage. Eddy-resolving simulations of the CO_2 flux and associated biogeochemical fields in the Drake Passage region are presented in section 3 using cross correlation and eddy-centric analysis. The influence of mesoscale eddies on the CO_2 flux and nutrient supply are summarized and discussed in section 4. We conclude in section 5.

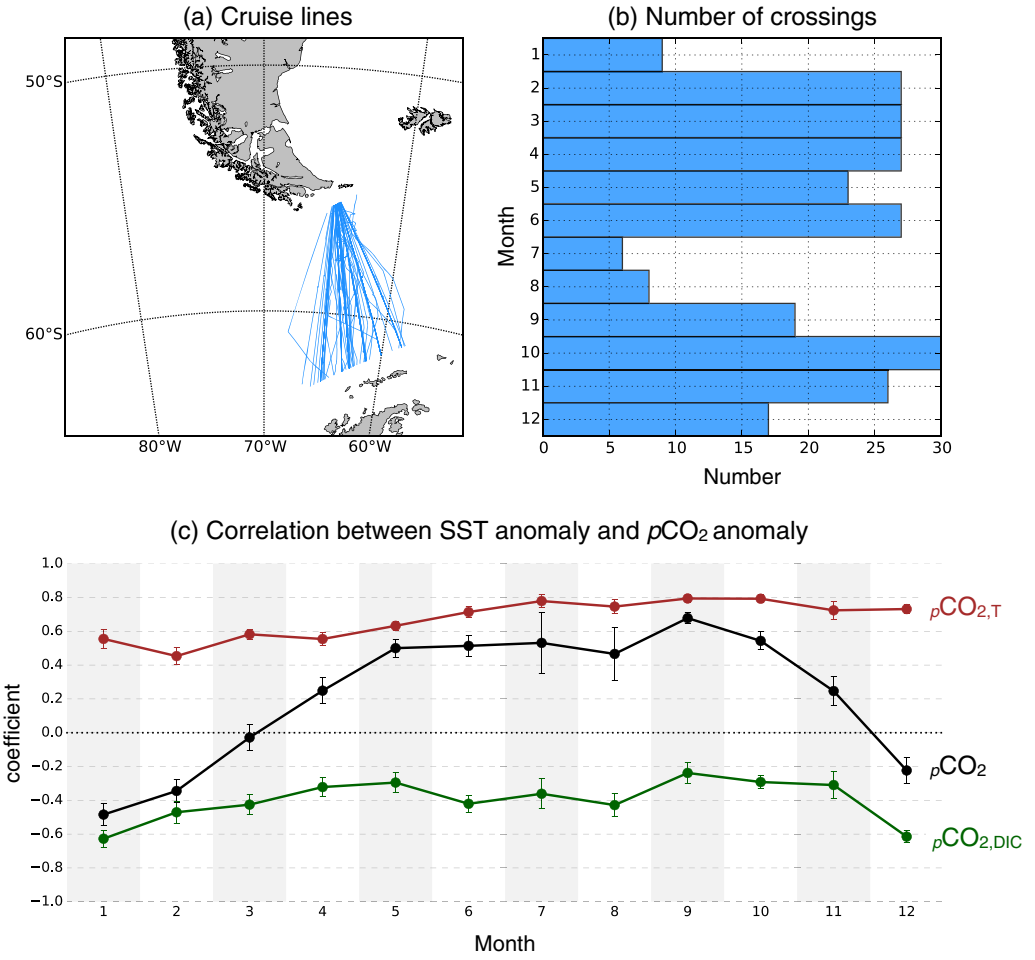

Figure 1. (a) Cruise lines across the Drake Passage along which repeat measurements were taken during the period 2002–2015, (b) number of crossings for each month and (c) the cross correlation between SST and pCO_2 anomalies. Correlation coefficients are computed using anomalies along the transect and are grouped by month. Black dots and error bars in Figure 1c represent the mean and standard error. The pCO_2 is separated into temperature-driven ($pCO_{2,T}$) and DIC-driven ($pCO_{2,DIC}$) contributions following *Munro et al.* [2015b]. The correlation between SST and $pCO_{2,T}$ (red) and $pCO_{2,DIC}$ (green) anomalies is plotted.

2. Analysis of Observations in Drake Passage

2.1. Data From the *Laurence M. Gould*

We use the sea surface temperature (SST) and the pCO_2 in surface waters sampled from the Antarctic Research Supply Vessel (ARSV) *Laurence M. Gould* across the Drake Passage during the period 2002–2015 [*Jiang et al.*, 2014; *Munro et al.*, 2015a,2015b] (Figure 1a). This data set includes 246 crossings of Drake Passage with at least some measurements in every month of the year; crossings are most frequent in October (30 times in the austral spring) and least frequent in July (6 times in the austral winter) over the length of the time series (Figure 1b). The cross correlation between SST and pCO_2 anomalies are of interest in the investigation of the role of mesoscale structures on pCO_2. Hence, the linear trend of the surface data along the crossing is removed to reveal anomaly patterns. The result is qualitatively the same if other plausible methods are used in the computation of anomalies (Appendix A).

2.2. Observed Correlations Between SST and pCO_2 Anomalies

We investigate how the anomalies of physical and biogeochemical variables change associated with mesoscale eddies by examining the correlation near Drake Passage as shown in Figure 1c. The correlation coefficient between observed SST and pCO_2 anomalies is negative in summer (from December to March), suggesting anticyclonic warm eddies carry anomalously low pCO_2 water (Figure 1c). Interestingly, this relationship is reversed in austral winter with a positive correlation from April to November. Since the ocean

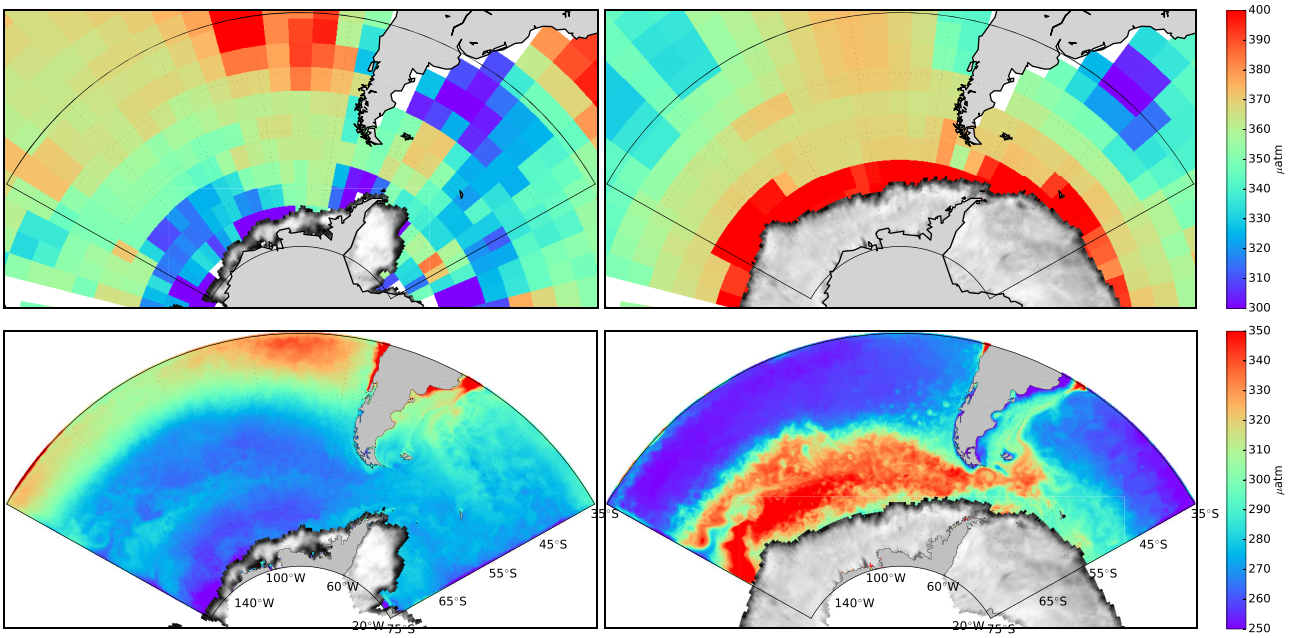

Figure 2. pCO_2 from the (a, b) climatology and (c, d) model simulation for (a, c) February and (b, d) August. Climatological oceanic pCO_2 data [*Takahashi et al*., 2014b] is adjusted to a reference year 2005 and, hence, systematically higher than the modeled pCO_2 for pre-industrial period. The color gray represents sea-ice from the model.

takes up CO_2 in summer due to increased primary production, the negative correlation suggests that more CO_2 enters the ocean in anticyclones than surrounding areas because of lower pCO_2. In winter, when the ocean emits CO_2 to the atmosphere, anticyclones release more CO_2 owing to their higher pCO_2. Cyclones exhibit the opposite behavior; less CO_2 uptake in summer and less outgassing in winter.

Such relationships are also seen in the analysis of expendable bathythermograph (XBT) data across the Drake Passage. For example *Sprintall et al*. [2012] found that warmer waters have greater ΔpCO_2 (air-sea) in spring north of 57°S associated with the decrease of oceanic pCO_2. In winter, XBT data show a negative correlation between temperature and ΔpCO_2 south of the Polar Front, corresponding to higher oceanic pCO_2 in warmer water. *Sprintall et al*. [2012] attribute this seasonal change in correlation to variation in the relative impacts of temperature-driven solubility and biological uptake, similar to what we will describe in section 4.1. In order to probe the mechanisms linking hydrodynamic variability with air-sea CO2 flux, we now turn to a high resolution model of a section of the Antarctic Circumpolar Current.

3. Coupled Eddying Biogeochemical-Physical Model of the Drake Passage Region

3.1. High Resolution Model Including Drake Passage

The oceanic carbon cycle is simulated by accounting for oceanic transport as well as biological and carbonate sources/sinks. Here physical fields taken from the MIT Ocean General Circulation Model (MITgcm) [*Marshall et al*., 1997a,1997b; *Adcroft et al*., 1997; *Marshall et al*., 1998; *Adcroft et al*., 1999] are used to drive a carbon cycle model. The model is configured in a sector of the Antarctic Circumpolar Current including the Drake Passage with a horizontal resolution of 1/20° and 50 vertical levels. The model domain also encompasses the region of the *Laurence M. Gould* transects. Forcing data sets for the model are the corrected normal year Common Ocean-ice Reference Experiments version 2 (CORE-II) [*Large and Yeager*, 2009] at the surface and OCean Comprehensible Atlas (OCCA) product [*Forget*, 2010] at the open boundaries. This configuration is adopted from that described in *Tulloch et al*. [2014] where the simulated physical solution is intensively evaluated against observations.

The biogeochemical sources and sinks for the carbon cycle are air-sea CO_2 flux, carbonate flux and primary production. They are computed using a simple biogeochemical model [*Dutkiewicz et al*., 2005; *Parekh et al*., 2006; *Verdy et al*., 2007] which simulates 6 biogeochemical variables: DIC, alkalinity, oxygen, nitrate (NO_3)

Table 1. Parameter Names, Values, and Units for the Biogeochemical Model

Parameter Name	Value	Units
Light		
Light attenuation coefficient (k_l)	0.02	m^{-1}
Self-shading coefficient (k_{Chl})	0.02	$m^2\ mg^{-1}$
Photosynthetically active radiation	0.4	Dimensionless
Half saturation light constant	30	$W\ m^{-2}$
Net Community Productivity		
Maximum consumption rate (α)	0.84	$\mu M\ month^{-1}$
Half saturation NO_3 constant (k_{NO_3})	8	μM
Half saturation Fe constant (k_{Fe})	0.12	nM
Fraction of new production to DON pool	0.7	Dimensionless
Time scale for DON remineralization	3	month
N:Fe stoichometry	0.007	Dimensionless
Iron		
Scavenging rate	0.2×10^{-7}	s^{-1}
Ratio of sediment Fe to NO_3 flux (β)	1.153	Dimensionless
Minimum Fe flux from sediment ($F_{Fe,0}$)	1.0×10^{-5}	$pM\ s^{-1}$

and its dissolved organic form, and Fe. The model simulates net community production in the ocean using a combination of light and nutrient (Fe and NO_3) limitation. This is similar, but distinct from primary production which only includes the impact of autotrophs (described in Appendix B). The biogeochemical model was integrated for 3 years from an initial state taking monthly mean boundary conditions from a global model. Model parameters are tuned to yield biogeochemical states close to the climatology. A list of parameter values is given in Table 1. The simulated surface pCO_2 captures seasonal changes of the meridional pCO_2 gradient in the climatology: increasing/decreasing pCO_2 toward the equator in summer/winter (Figure 2). More evaluation of the modeled biogeochemistry against the climatology and observation is provided in Appendix D.

3.2. Simulations of Air-Sea CO_2 Flux

The air-sea CO_2 flux (F_{CO_2}) is parameterized as

$$\begin{aligned} F_{CO_2} &= K_w(1-A_{SI})(pCO_2{}^{atm}-pCO_2) \\ &= K_w(1-A_{SI})\Delta pCO_2, \end{aligned} \tag{1}$$

where K_w is the gas transfer velocity ($m\ s^{-1}$) estimated using wind speed squared and SST [*Wanninkhof*, 1992]. K_w is then inversely scaled by the sea-ice coverage (A_{SI}) in each grid cell and becomes zero when the grid cell is completely covered by sea-ice. The atmospheric pCO_2 ($pCO_2{}^{atm}$) is set to a pre-industrial level (278 ppmv), and the oceanic pCO_2 at the surface (pCO_2) is calculated following *Follows et al*. [2006]. A positive F_{CO_2} means that the ocean receives CO_2 from the atmosphere, and vice versa.

3.3. Analysis of Model Results

3.3.1. Eddy Correlations Over the Seasonal Cycle

The correlation between simulated SSH and pCO_2 anomalies (solid black line in Figure 3) exhibits similar behavior to that found in the data described in section 2 (compare to Figure 1c). In summer, the pCO_2 anomaly is negatively correlated with the SSH anomaly, indicating that anticyclones/cyclones have lower/higher oceanic pCO_2. However, the correlation changes the sign to become positive in winter: anticyclones have higher pCO_2 and cyclones lower pCO_2. Higher pCO_2 indicates either less CO_2 uptake in summer, or more outgassing in winter, explaining the correlation between anomalies of SSH and CO_2 flux (orange line in Figure 3). A positive correlation in summer suggests that warm/cold anticyclonic/cyclonic eddies have higher/lower CO_2 flux into the ocean. In winter, anticyclones/cyclones release more/less CO_2 into the atmosphere than their surroundings.

Correlations between SSH anomaly and other biogeochemical variables are robust throughout the year. DIC and NO_3 anomalies are negatively correlated with SSH anomalies (light blue and red lines, respectively, in Figure 3), suggesting that anticyclones/cyclones have lower/higher DIC and NO_3. On the other hand, Fe and community productivity have positive correlations with SSH anomalies (purple and green lines, respectively, in Figure 3), indicating that enhanced levels of Fe and more community productivity occurs in anticyclones. Since the Fe is the limiting nutrient in most of the model domain in the SO (see Appendix D), it is understandable that Fe and community productivity anomalies show a similar relationship with mesoscale eddies.

3.3.2. Biogeochemical Fields Using Eddy-Centric Analysis

We compute the mean anomalies of biogeochemical variables using an eddy-centric coordinate. Using total SSH fields, we identified 1268 anticyclones and 1624 cyclones with lifetimes longer than 20 days over 2 years (Appendix C). The eddy-centric composite average of the CO_2 flux anomalies changes sign with SSH

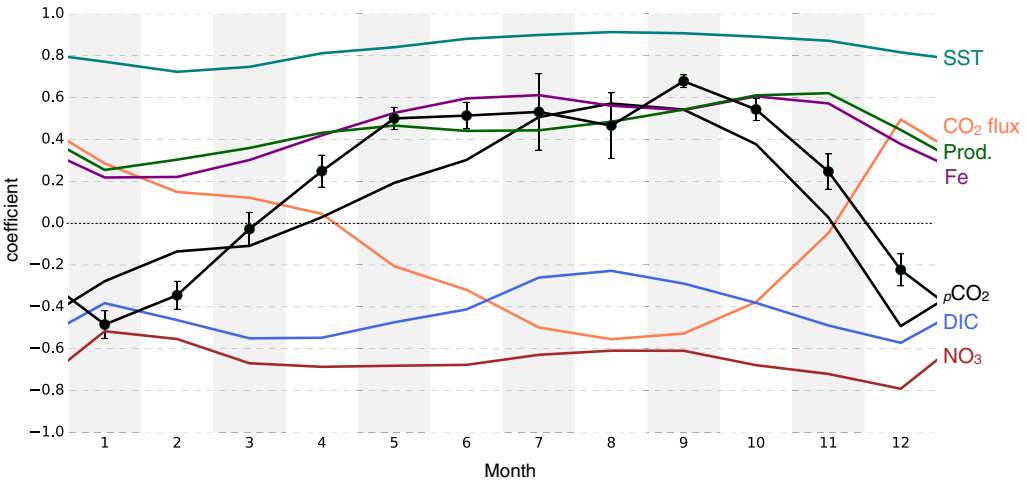

Figure 3. Solid lines are the modeled monthly averaged cross correlation coefficients of SST (teal), CO_2 flux (orange), net community productivity (green), Fe (purple), pCO_2 (black), DIC (light blue) and NO_3 (red) with the SSH anomaly associated with mesoscale eddies identified in our numerical model. The monthly averaged correlation coefficients are computed using spatially averaged anomalies of SSH and biogeochemical variables from all mesoscale eddies for each month. The solid line with dots is the mean correlation coefficient between SST and pCO_2 across the Drake Passage from *Laurence M. Gould* as shown in Figure 1.

anomaly in different seasons (Figures 4a–4d), as revealed by the cross correlation in section 3.3.1. The composite average of CO_2 flux has a monopole structure and the maximum anomaly can be found within a circle of radius L_s whose size is the same as the one enclosed by SSH contour with the maximum mean current speed. The CO_2 flux anomalies are the largest in winter. Anomalous pCO_2 in mesoscale eddies influences the CO_2 flux anomalies in all seasons. A positive anomaly of pCO_2 leads to less CO_2 uptake in summer and more outgassing in winter and thus a negative anomaly of CO_2 flux. On the other hand, a negative pCO_2 anomaly results in a positive CO_2 flux anomaly. Since the ocean receives CO_2 in summer but emits in winter, the CO_2 flux anomaly indicates that anticyclones/cyclones take up more/less CO_2 in summer and releases more/less CO_2 in winter. If one takes the modification of wind speed by warm/cold eddies into account [*Frenger et al*., 2013], the CO_2 flux anomaly can be amplified. It should be noted that the interaction between SST and wind speed is not simulated in this study.

Variability of DIC on the mesoscale does not show a seasonal dependence (Figures 4i–4l). Anticyclones and cyclones have lower and higher DIC levels, respectively, than the spatial mean in both summer and winter. The DIC concentration generally increases with depth (Figure 5) and so the downward/upward displacement of isopycnals in anticyclones/cyclones results in a negative/positive DIC anomaly in both seasons. DIC has a negative meridional gradient, decreasing toward the north (Figure 5). Because the gradient of DIC across the Antarctic Circumpolar Current is negative, eddy fluxes across the front can yield negative correlation between SSH and DIC anomalies through the so-called "trapping" mechanism. Specifically, this effect is produced by lateral cross-frontal transport of warm anticyclonic eddies (cold cyclonic eddies) with low (high) DIC from the north (south) to the south (north).

Net community productivity is enhanced in anticyclones and reduced in cyclones in all seasons (Figures 6a–6d). The composite averages of the net community productivity anomaly have a sign opposite to that of the NO_3 anomaly (Figures 6e–6h), but the same sign as the Fe anomaly (Figures 6i–6l), reflecting the Fe-limited environment. The NO_3 spatial distribution is similar to that of DIC (Figure 5), suggesting that vertical isopycnal displacement and the trapping mechanism are both potentially at work in shaping the NO_3 anomalies. The Fe spatial distribution is quite different from those of DIC and NO_3 and its anomalies are not entirely determined by these two mechanisms, as will be discussed in section 4.2.

4. Proposed Mechanisms

4.1. Seasonal Cycle of CO_2 Flux Anomalies

Both observed and simulated mesoscale variabilities of pCO_2 show the same seasonal dependence as presented in section 3.3.1. Why does the correlation between anomalies of SST (or SSH) and pCO_2 reverse with

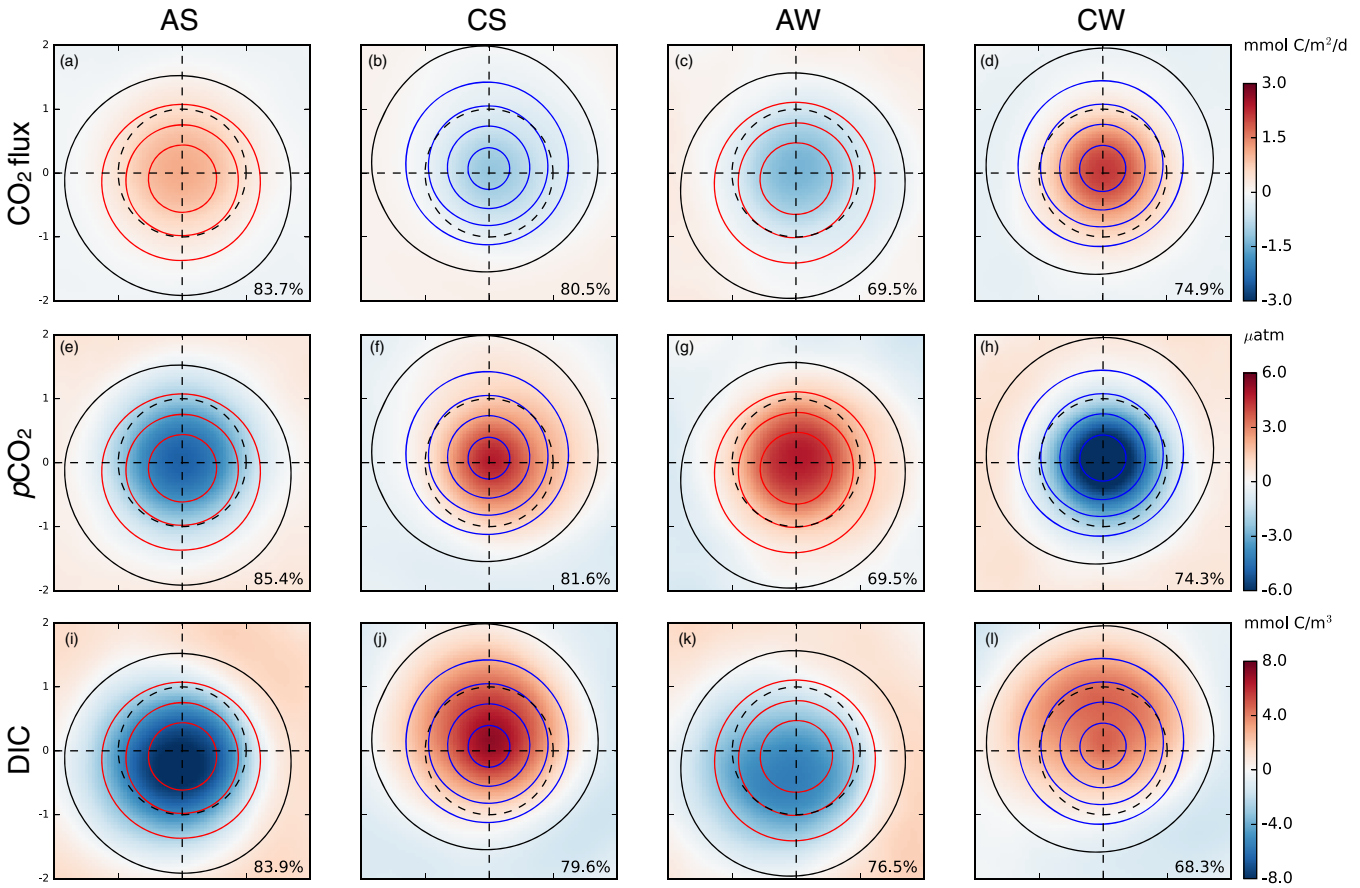

Figure 4. Eddy-centric composite averages for anomalies of (a–d) CO_2 flux (e–h) pCO_2 and (i–l) DIC. From the left to right, columns represent anticyclones in summer, cyclones in summer, anticyclones in winter and cyclones in winter. Eddies are mapped on the eddy-centric coordinate spanning $\pm 2L_s$, hence the dashed circle with a unit radius corresponds to one with a radius of L_s. Red, blue and black contours represent positive, negative and zero SSH anomalies with a 5 cm interval, respectively. The numbers on the lower right corner are the percentage of eddies whose anomaly have the same sign as the composite average.

season? We partitioned pCO_2 into the temperature-driven ($pCO_{2,T}$) and DIC-driven ($pCO_{2,DIC}$) components for both observation and model following *Takahashi et al.* [2002], *Jiang et al.* [2014] and *Munro et al.* [2015b] and investigate the seasonality of mesoscale variability of pCO_2.

Observations suggest that anomalies of $pCO_{2,T}$ and SST are positively correlated throughout the year (red line in Figure 1c), indicating that warmer temperature in anticyclones increases pCO_2 because of reduced solubility. In contrast, cyclones with colder temperature have higher solubility and lower pCO_2. On the other hand, $pCO_{2,DIC}$ are negatively correlated with the SST anomaly (green line in Figure 1c). This suggests that anomalously low and high pCO_2 are expected in anticyclones and cyclones, respectively, owing to changes in DIC. Hence the observed seasonal variability of the correlation between anomalies of SST and pCO_2 results from a change in the balance between $pCO_{2,T}$ and $pCO_{2,DIC}$. In summer, the modulation of pCO_2 by anomalous temperature in eddies is weaker than that by anomalous DIC, and the mesoscale variabilities of pCO_2 and CO_2 flux are governed by anomalous aqueous CO_2 of DIC. In winter, however, the temperature-driven component dominates the pCO_2 and CO_2 flux anomalies.

Model simulations confirm relationships seen in the observations. The $pCO_{2,T}$ and SSH anomalies are positively correlated in both summer and winter (Figures 7a–7d). Warm eddies have low solubility, hence pCO_2 increases, leading to a positive correlation between $pCO_{2,T}$ and SSH. The $pCO_{2,DIC}$ is negatively correlated with SSH anomaly (Figures 7e–7h). The inverse relationship between $pCO_{2,DIC}$ and SSH can be anticipated from the negative correlation between DIC and SSH anomalies (Figures 3 and 4i–4l)).

The eddy-centric analysis clearly shows that the balance between temperature and DIC tendencies varies (Figure 7). In summer, the $pCO_{2,DIC}$ anomaly is greater and more robust than the $pCO_{2,T}$ anomaly, resulting

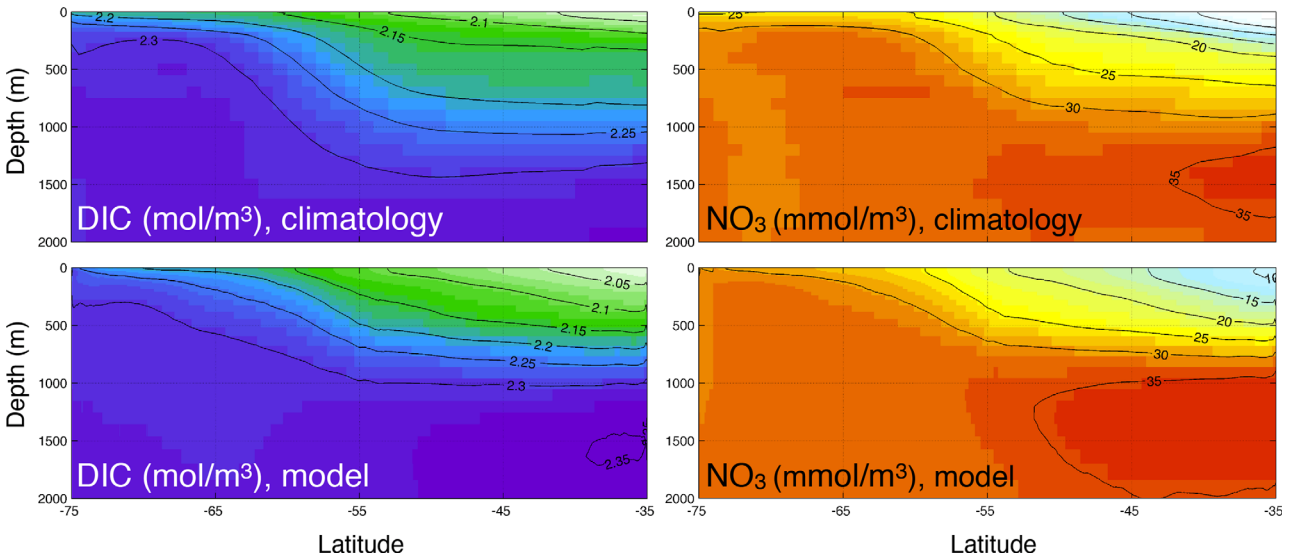

Figure 5. The zonal mean DIC and NO_3 from (top) the World Ocean Atlas 2009 climatology and (bottom) biogeochemical model.

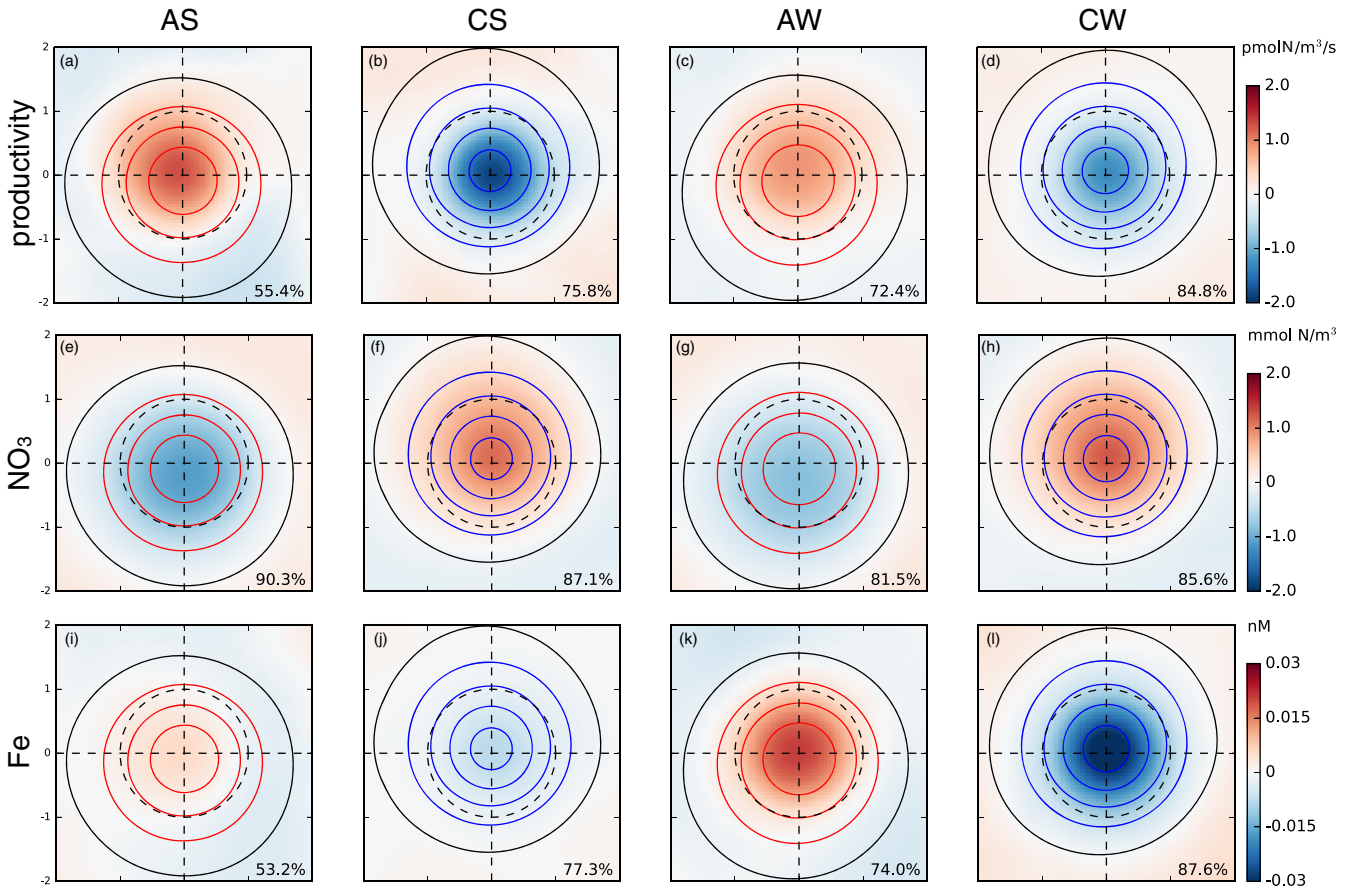

Figure 6. Eddy-centric composite averages for anomalies of (a–d) surface net community productivity (e–h) NO_3 and (i–l) Fe. From the left to right, columns represent anticyclones in summer, cyclones in summer, anticyclones in winter and cyclones in winter. Eddies are mapped on the eddy-centric coordinate spanning $\pm 2L_s$, hence the dashed circle with a unit radius corresponds to one with a radius of L_s. Red, blue and black contours represent positive, negative and zero SSH anomalies with a 5 cm interval, respectively. The numbers on the lower right corner are the percentage of eddies whose anomaly have the same sign as the composite average.

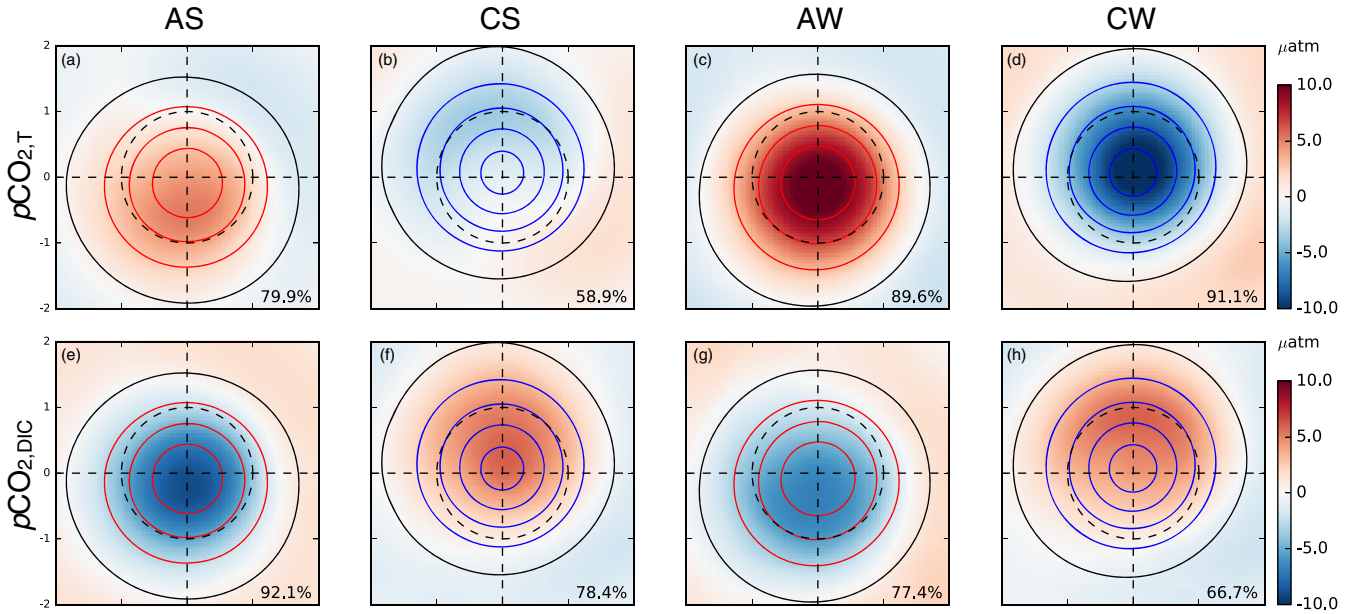

Figure 7. Eddy-centric composite averages for anomalies of (a–d) temperature-driven pCO_2 and (e–h) DIC-driven pCO_2. From the left to right, columns represent anticyclones in summer, cyclones in summer, anticyclones in winter and cyclones in winter. Eddies are mapped on the eddy-centric coordinate spanning $\pm 2L_s$, hence the dashed circle with a unit radius corresponds to one with a radius of L_s. Red, blue and black contours represent positive, negative and zero SSH anomalies with a 5 cm interval, respectively. The numbers on the lower right corner are the percentage of eddies whose anomaly have the same sign as the composite average.

in a negative correlation between pCO_2 and SSH anomalies. In winter, on the other hand, the $pCO_{2,T}$ anomaly dominates the DIC effect on pCO_2, leading to a positive correlation. The changes in the balance can be understood using anomalies in the eddy centric composite averages. One can estimate effects on pCO_2 due to SST, DIC and alkalinity (Alk) changes thus:

$$\frac{\Delta pCO_2}{pCO_2} \approx \frac{1}{pCO_2}\frac{\partial pCO_2}{\partial T}\Delta T + \frac{1}{pCO_2}\frac{\partial pCO_2}{\partial DIC}\Delta DIC + \frac{1}{pCO_2}\frac{\partial pCO_2}{\partial Alk}\Delta Alk$$
$$= \beta \Delta T + \gamma_{DIC}\frac{\Delta DIC}{DIC} + \gamma_{Alk}\frac{\Delta Alk}{Alk}, \quad (2)$$

when salinity changes are small [*Takahashi et al.*, 1993; *Mahadevan et al.*, 2004; *Sarmiento and Gruber*, 2006; *Lovenduski et al.*, 2007; *Merlivat et al.*, 2015]. β is close to $0.0423^{\circ}C^{-1}$, and γ_{DIC} and γ_{Alk} are the Revelle factor and alkalinity factor that are approximately 12 ± 0.5 and -11 ± 0.5 in the Drake Passage, respectively [*Takahashi et al.*, 2014a]. In the open Southern Ocean, changes driven by alkalinity perturbation are smaller than the other two terms and have an insignificant contribution to ΔpCO_2, while its contribution can be significant in other ocean regions (e.g., North Atlantic) [*Takahashi et al.*, 2014a]. Our analysis also shows that the impact of alkalinity on pCO_2 is insignificant (not shown). If we drop off the last term on the right-hand-side, equation (2) indicates that the sign of ΔpCO_2 in mesoscale eddies is determined by the sum of weighted SST and DIC anomalies. As shown in Figures 4i–4l, anticyclonic eddies are characterized by warmer SST and lower DIC concentrations. Cyclonic eddies, by contrast, have colder SSTs and higher DIC concentrations. On the mesoscale, SST and DIC anomalies averaged over the circular area with the radius L_s vary by season (Table 2). SST anomalies are larger in winter while DIC anomalies are larger in summer. Inserting these values in equation (2) for anticyclones in Table 2 results in negative

Table 2. Spatially Averaged Eddy Composite Averages of SST Anomaly, DIC Anomaly and DIC Concentration in Anticyclones and Cyclones in Summer and Winter

	Summer		Winter	
	Anticyclone	Cyclone	Anticyclone	Cyclone
ΔSST (°C)	0.37	−0.20	0.76	−0.71
ΔDIC (mmol C/m^3)	−5.91	4.46	−3.88	3.23
DIC (mol C/m^3)	2.09	2.12	2.10	2.13

[a]The circular area with the radius L_s is considered in the spatial average.

Table 3. Normalized Vertical Gradient ($\times 10^{-3}$) at the Base of the Mixed Layer Depth

	Summer		Winter	
	Anticyclone	Cyclone	Anticyclone	Cyclone
NO_3	−0.31	−0.47	−1.68	−1.29
Fe	−9.86	−9.31	−7.38	−7.83

ΔpCO_2 in summer but positive in winter. In contrast, ΔpCO_2 in cyclones becomes positive in summer but negative in winter. Hence, the seasonal change of correlation coefficient between SSH and pCO_2 anomalies is the consequence of the seasonally varying magnitude in the anomaly of SST and DIC.

4.2. Responses in Nitrate and Iron

It is interesting to note that simulated NO_3 and Fe have opposite-signed anomalies in both summer and winter (Figures 6e–6l): anticyclones have anomalously high Fe but low NO_3, and cyclones have anomalously low Fe and high NO_3. Why do they display different responses driven by the same physical processes?

Mesoscale eddies displace vertical isopycnals and modulate the surface NO_3. Doming of isopycnals in cyclones shoals subsurface water abundant with NO_3 and creates a positive anomaly. The opposite is true for anticyclones. Downward displacement of isopycnal in anticyclones results in a negative NO_3 anomaly. The trapping mechanism can also be applied to explain the NO_3 anomalies seen in the eddy-centric composite average in Figures 6e–6h. The meridional overturning circulation and the Fe-limited environment in the SO set up warm water with low NO_3 in the north and cold water with high NO_3 in the south. Mesoscale eddies can trap water parcels and transport them horizontally to other regions with different environments. If this trapping mechanism is at work, warm anticyclonic eddies should carry waters with low NO_3 and cold cyclonic eddies waters with high NO_3 across the Antarctic Circumpolar Current.

Similar to NO_3, Fe concentration increases with depth near the surface. As such, isopycnal displacements by mesoscale eddies would tend to produce the same sign of Fe anomalies as for NO_3. However, Figures 6i–6l show the anomalies with the opposite sign, indicating other processes are at work.

In order to evaluate the potential role of trapping, we examined the meridional gradient of Fe using the data described in *Tagliabue et al*. [2014]. Although Fe concentration can be elevated near the shelf with sedimentary sources, Fe is mostly depleted at the surface in the open ocean. Dust input increases Fe concentration in the lee of the continent while intense vertical mixing at the north of ACC in winter supplies Fe to the surface ocean. However these sources are limited to specific regions and Fe is quickly used up by biological activity when light is available. All these complex sources and sinks make it difficult to anticipate the effect of trapping on the composite average of Fe anomaly, which leads us to consider the role of vertical mixing.

The vertical diffusion of a tracer depends on the vertical diffusivity and the vertical gradient of that tracer. Since the same vertical diffusivity is applied to both NO_3 and Fe, it is the vertical gradient of the nutrients that creates the different responses.

We computed the vertical gradient of nutrients at the base of the surface mixed layer and normalized it by their concentration below the mixed layer. The normalized vertical gradients are all negative, suggesting that vertical mixing supplies nutrients to the surface mixed layer (Table 3). However, the effect of vertical mixing for NO_3 is not strong enough to overcome the influence of the trapping and isopycnal displacement mechanisms. The normalized vertical gradient of Fe is one order of magnitude greater than that of NO_3. Fe is the limiting nutrient in most of the eddy areas and becomes close to depletion when the productivity is high. As a result, the vertical gradient for Fe is greater than NO_3 and so vertical mixing of Fe is likely to have greater impact. Although the simulated vertical gradients of nutrients can slightly differ from the climatology, the observed vertical gradient of Fe [*Tagliabue et al*., 2014] is still greater than that of NO_3 from World Ocean Atlas 2009 climatology at the upstream of Drake Passage (not shown).

Even though the normalized vertical gradients of Fe are similar between anticyclones and cyclones, the simulated vertical diffusivity is much greater in anticyclones than in cyclones [see *Song et al*., 2015, Figure 3]. A variety of processes may contribute to differences in the mixing environments within cyclonic and anticyclonic eddies. For example, warm anticyclonic eddies become less stable after losing buoyancy to the atmosphere more quickly [e.g., *Williams*, 1988]. Also, the trapping of near-inertial waves promotes more vertical mixing [*Kunze*, 1985; *Kunze et al*., 1995]. The weaker stratification also helps the wind energy to penetrate deeper level [*Koszalka et al*., 2010].

5. Conclusion

We investigated the mesoscale modulation of CO_2 flux and biogeochemical variables using both observations across the Drake Passage and an eddy-resolving numerical ocean model configured in the Drake Passage region. The 13 years (2002–2015) of SST and oceanic pCO_2 observations with 246 crossings are grouped by months after removing the linear trend across the Drake Passage. We computed the cross correlation between SST and pCO_2 anomalies to examine the observed mesoscale modulation. Using the eddy detection algorithm, more than 2800 eddies with lifetimes longer than 20 days were identified from the numerical model output and averaged after projecting to eddy-centric coordinate.

The cross correlation between SST and pCO_2 anomalies reveals a marked seasonal variability: negative correlation in summer and positive correlation in winter in both observations and model. The change in correlation over the seasons suggests that anticyclones are more active in both taking up CO_2 in summer and releasing CO_2 into the atmosphere in winter. Cyclones are less active than surrounding waters and behave in the opposite sense to anticyclones.

pCO_2 in the ocean changes with both physical and biogeochemical processes. The mesoscale modulation of CO_2 flux is thus determined by the balance between temperature-driven and DIC-driven effects. Warming of the surface ocean reduces the solubility, hence the pCO_2 increases. Warmer SST in anticyclones thus leads to the pCO_2 increase and either to less CO_2 uptake in summer or more outgassing in winter. Anomalously low DIC in anticyclones reduces pCO_2 leading to either more uptake in summer or less outgassing in winter. In summer, the DIC-driven effect is greater than the temperature-driven effect, resulting in a negative correlation between SST and pCO_2 anomalies. In winter, however, the oceanic pCO_2 is governed by the temperature-driven effect, yielding a positive correlation.

Another interesting finding from the model analysis is the different responses of nutrients to the same physical processes associated with mesoscale eddies. The vertical displacement of isopycnals and trapping mechanism result in higher/lower NO_3 concentration in cyclones/anticyclones with increasing NO_3 concentration toward the pole and depth. Although Fe concentration increases with depth, its anomalies have the sign opposite to NO_3, suggesting that the vertical displacement of isopycnals does not shape the anomalies. The meridional gradient of Fe is not as clear as NO_3, making the response of trapping mechanism complicated.

A hydrodynamic model simulation similar to that described here shows anomalous vertical mixing in mesoscale eddies [*Song et al*., 2015]. From the present solutions we infer that stronger vertical mixing in deeper mixed layers in anticyclones supplies Fe from the subsurface, resulting in a positive anomalies. Cyclones are characterized by weaker vertical mixing, shallower mixed layers, and negative Fe anomalies. The footprint of vertical mixing modulation by eddies, however, is not apparent in NO_3 anomalies. The two nutrients differ in their responses to the same vertical mixing as their vertical gradients at the base of the surface mixed layer are significantly different. As Fe is the limiting nutrient in the most of Southern Ocean, surface depletion creates a greater vertical gradient than for NO_3. NO_3, on the other hand, is not fully utilized near the surface, which reduces its vertical gradient. As a result, the same vertical mixing creates vastly different fluxes for these two nutrients, bringing about mesoscale anomalies of opposite sign.

The observations show that temperature-driven and DIC-driven pCO_2 are out of phase and compensate one-another, resulting in smaller seasonal variability of pCO_2. The compensation also occurs at the mesoscale and shapes the seasonality of mesoscale modulation on CO_2 flux. The strong seasonality of mesoscale variability of CO_2 flux suggests that an important mesoscale signal may be lost in annual averages.

Appendix A: Anomaly Computation

The anomalies of SST and pCO_2 were obtained after removing the linear trend of each crossing across the Drake Passage in this study. This separates an anomaly pattern from the sampled SST data if the meridional trend can be depicted by a linear function (Figure A1a). However, this technique may not be optimal for pCO_2 whose meridional gradient is not always linear. Indeed, the pCO_2 climatological mean distribution across the Drake Passage is not linear (Figure A1b). We therefore experimented by removing a quadratic trend and monthly mean.

The seasonality of cross correlation coefficients is robust regardless the methods for anomaly computation. Correlation coefficients between SST and pCO_2 remain negative in austral summer and positive in austral

winter (Figure A1c). The seasonality becomes weak when the monthly mean was removed to compute the anomaly, but the timing when the coefficient changes sign remains the same. The anomaly computation for model data is explained in Appendix C.

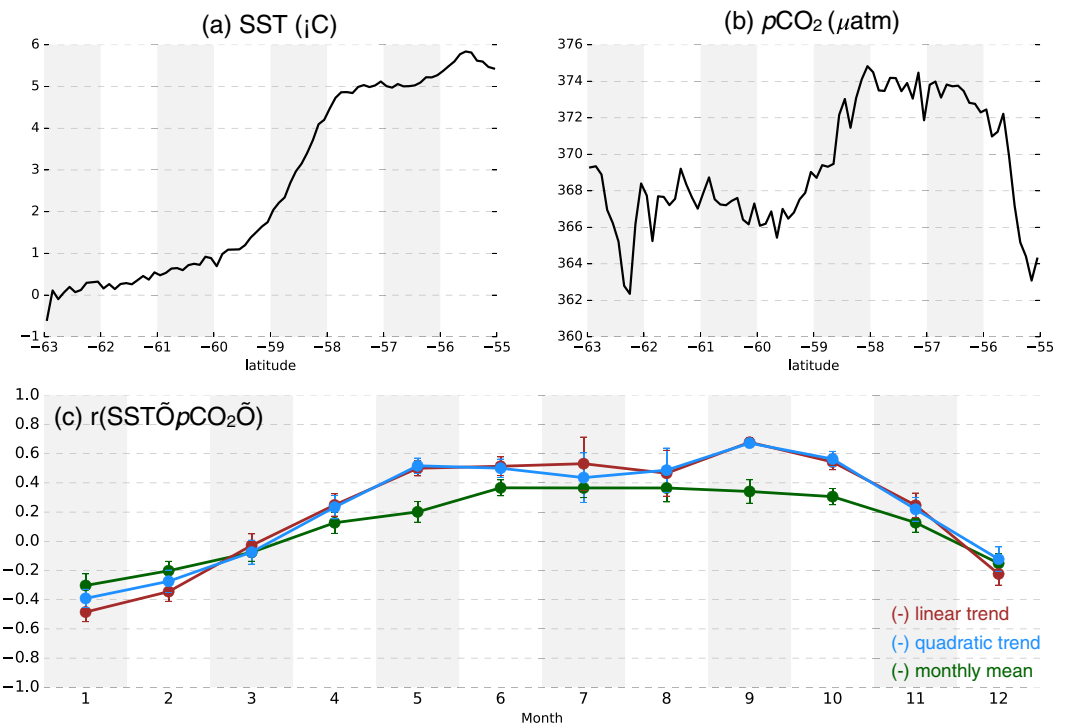

Figure A1. (a) Climatological mean SST, (b) pCO_2 across the Drake Passage during the period 2002–2015, and (c) cross-correlation coefficients between SST and pCO_2 anomalies when anomalies are computed with respect to the linear trend (brown), the quadratic trend (sky blue) along the Drake Passage and the monthly mean (dark green). The monthly mean was computed after grouping data for each month and latitude. The error bars in (c) represent the standard error.

Appendix B: Biogeochemical Model

The carbon cycle is simulated using a simple biogeochemical model, the DIC package in MITgcm. The CO_2 air-sea flux (F_{CO_2}) acts as a source/sink term in the equation for dissolved inorganic carbon (DIC) in the model.

$$\frac{\partial \mathrm{DIC}}{\partial t} = -\nabla \cdot (\mathbf{u}\mathrm{DIC}) + \kappa \frac{\partial^2 \mathrm{DIC}}{\partial z^2} + F_{CO_2} + R_{C:N} S_{NO_3} + S_C, \tag{B1}$$

where **u** is a vector that represents the three-dimensional velocity field, κ is the vertical diffusivity, $R_{C:N}$ is the Redfield ratio between carbon and nitrogen, S_{NO_3} is the contribution from biological production and remineralization, and S_C is the source term associated with calcium carbonate flux. The vertical mixing of the biogeochemical variables is estimated by the nonlocal K-Profile Parameterization (KPP) scheme [*Large et al.*, 1994].

The biological uptake of inorganic nutrients is parameterized as a function of light, NO_3 and Fe.

$$B = \alpha \frac{I}{I + k_I} \min\left(\frac{NO_3}{NO_3 + k_{NO_3}}, \frac{Fe}{Fe + k_{Fe}}\right), \tag{B2}$$

where α is maximum uptake rate, k_I, k_{NO_3} and k_{Fe} are the half saturation values for light (I), NO_3 and Fe, respectively. The uptake of inorganic matter is subsequently divided between a dissolved organic pool in the surface waters and the fraction exported to depth and remineralized. B can thus be likened to "community production" as it includes the impact of herbivores as well as primary producers. This is similar, but distinct from primary production which only includes the impact of autotrophs.

The light decays exponentially with the e-folding scale of $(k + Chl \times k_{Chl})$ where k is the light attenuation coefficient by water molecules, Chl is the chlorophyll concentration and k_{Chl} accounts for the absorption of

light by chlorophyll [*Song et al.*, 2016]. We used the annual mean of SeaWiFS chlorophyll concentration for *Chl*. Fe has two sources: aeolian dust from the data set by *Luo et al.* [2008], and the sediments parameterized following *Elrod et al.* [2004]. A list of parameter values is given in Table 1.

Appendix C: Eddy Centric Analysis

The first step for the eddy centric analysis is to detect eddies. We closely followed the procedure presented in *Chelton et al.* [2011] and *Song et al.* [2015] for the identification of well-formed eddies using the SSH field. The detection algorithm searches for the closed SSH contours and determines whether they are eddies by going through the criteria given in *Song et al.* [2015]. The detected eddies and their trajectory are plotted in Figure C1a.

For each eddy, we estimate the radius L_s whose circle has the same size as the closed SSH contour with the maximum mean current speed. Then V, the subset of a variable of interest ranging from $-2.5L_s$ to $2.5L_s$ around the eddy center, is extracted and its anomaly V' is computed as $V' = V - [V]$, where $[V]$ represents the regression plane. The mean L_s is approximately 45 km, hence the mean subset size is 225 km $\times$ 225 km. The anomaly V' is mapped onto the eddy-centric coordinate spanning $\pm 2L_s$, and 4 composite averages were then computed: anticyclones and cyclones in austral summer (December - March) and austral winter (June - September).

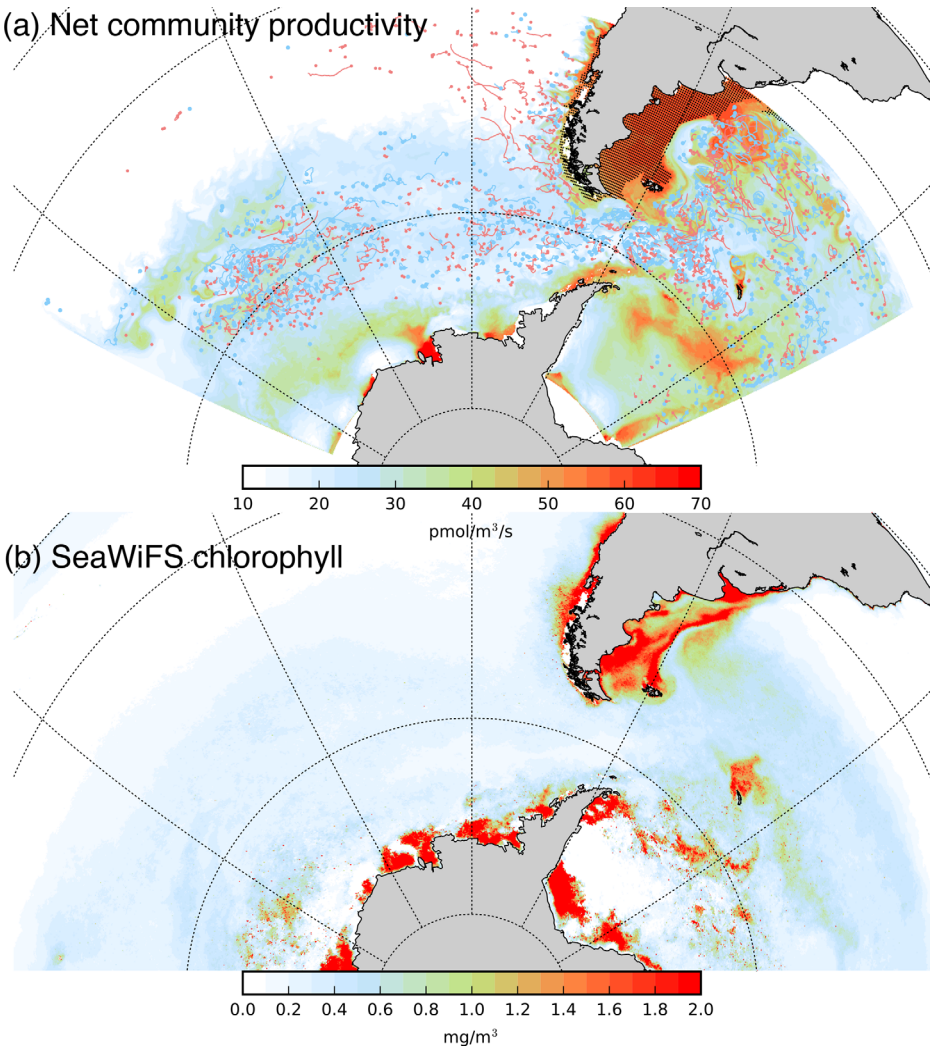

Figure C1. (a) Biological production simulated by the biogeochemical model and (b) the chlorophyll biomass from the SeaWiFS data set averaged over December and January. The Patagonian shelf region with black dots in Figure C1a is where biological production is limited by NO_3 in the model. Light blue and red dots represent the initial location of cyclonic and anticyclonic eddies who live more than 20 days, respectively, and lines are their trajectories.

Appendix D: Model Evaluation

Although the biogeochemical model for carbon flux is relatively simple, it captures the observed large scale features of biogeochemical ocean states. The zonal mean of DIC and NO_3 are close to World Ocean Atlas 2009 climatology (Figure 5). The simulated Fe level is also comparable to the observations upstream and across the Drake Passage (not shown).

Net community productivity displays a similar spatial pattern as that of the chlorophyll biomass measured from satellite. The model shows high production over the Patagonian Shelf and near the Antarctic in austral summer, which is in a good agreement with observed chlorophyll biomass spatial distribution (Figure C1). The simulated community activity is mainly limited by Fe in most areas of the model domain, except over the Patagonian shelf where NO_3 is the limiting nutrient. This is consistent with the observations presented in *Paparazzo et al*. [2010].

Acknowledgments
The authors thank Janet Sprintall and Teresa K. Chereskin (Scripps Institution of Oceanography) for useful discussions and two anonymous reviewers for their comments and suggestions. The MITgcm can be obtained from http://mitgcm.org. The surface forcing data used in this study are available at the Geophysical Fluid Dynamics Laboratory data portal webpage (http://data1.gfdl.noaa.gov/nomads/forms/core/COREv2.html). Resources supporting this work were provided by the NASA High-End Computing (HEC) Program through the NASA Advanced Supercomputing (NAS) Division at Ames Research Center with the award SMD-15-5752. HS, SD and JM were supported by the NSF MOBY project (OCE-1048926). SD also gratefully acknowledge the support of NSF OCE-1259388. DM and CS were supported by NSF (PLR-1341647, AOAS-0944761, and AOAS-066975) and the NOAA Climate Program Office (NA12OAR4310058). DJM gratefully acknowledges support by NSF (OCE-1048897) and NASA (NNX13AE47G). The pCO_2 data have been archived at CDIAC (cdiac.ornl.gov/ftp/oceans/VOS_-Gould_Lines/).

References

Adcroft, A., C. Hill, and J. Marshall (1997), Representation of topography by shaved cells in a height coordinate ocean model, *Mon. Weather Rev.*, *125*, 2293–2315.
Adcroft, A. J., C. N. Hill, and J. C. Marshall (1999), A new treatment of the Coriolis terms in C-grid models at both high and low resolutions, *Mon. Weather Rev.*, *127*, 1928–1936.
Boyd, P. W., et al. (2000), A mesoscale phytoplankton bloom in the polar Southern Ocean stimulated by iron fertilization, *Nature*, *407*(6805), 695–702.
Brix, H., K. I. Currie, and S. E. Mikaloff Fletcher (2013), Seasonal variability of the carbon cycle in subantarctic surface water in the South West Pacific, *Global Biogeochem. Cycles*, *27*, 200–211, doi:10.1002/gbc.20023.
Chelton, D. B., M. G. Schlax, and R. M. Samelson (2011), Global observations of nonlinear mesoscale eddies, *Prog. Oceanogr.*, *91*(2), 167–216, doi:10.1016/j.pocean.2011.01.002.
Cooper, D. J., A. J. Watson, and P. D. Nightingale (1996), Large decrease in ocean-surface CO2 fugacity in response to in situ iron fertilization, *Nature*, *383*, 511–513, doi:10.1038/383511a0.
Dufois, F., N. J. Hardman-Mountford, J. Greenwood, A. J. Richardson, M. Feng, and R. J. Matear (2016), Anticyclonic eddies are more productive than cyclonic eddies in subtropical gyres because of winter mixing, *Sci. Adv.*, *2*(5), e1600,282.
Dutkiewicz, S., A. Sokolov, J. Scott, and P. Stone (2005), A three-dimensional ocean-seaice-carbon cycle model and its coupling to a two-dimensional atmospheric model: Uses in climate change studies, in *Joint Program on the Sci. Policy Global Change, Rep*. 122, MIT Press, Cambridge, Mass.
Elrod, V. A., W. M. Berelson, K. H. Coale, and K. S. Johnson (2004), The flux of iron from continental shelf sediments: A missing source for global budgets, *Geophys. Res. Lett.*, *31*, L12307, doi:10.1029/2004GL020216.
Follows, M. J., S. Dutkiewicz, and T. Ito (2006), On the solution of the carbonate system in ocean biogeochemistry models, *Ocean Modell.*, *12*, 290–301.
Forget, G. (2010), Mapping ocean observations in a dynamical framework: A 2004-06 ocean atlas, *J. Phys. Oceanogr.*, *40*(6), 1201–1221.
Frenger, I., N. Gruber, R. Knutti, and M. Münnich (2013), Imprint of Southern Ocean eddies on winds, clouds and rainfall, *Nat. Geosci.*, *6*, 608–612, doi:10.1038/ngeo1863.
Gaube, P., D. B. Chelton, P. G. Strutton, and M. J. Behrenfeld (2013), Satellite observations of chlorophyll, phytoplankton biomass, and Ekman pumping in nonlinear mesoscale eddies, *J. Geophys. Res. Oceans*, *118*, 6349–6370, doi:10.1002/2013JC009027.
Gaube, P., D. J. McGillicuddy Jr., D. B. Chelton, M. J. Behrenfeld, and P. G. Strutton (2014), Regional variations in the influence of mesoscale eddies on near-surface chlorophyll, *J. Geophys. Res. Oceans*, *119*, 8195–8220, doi:10.1002/2014JC010111.
Gruber, N., et al. (2009), Oceanic sources, sinks, and transport of atmospheric CO_2, *Global Biogeochem. Cycles*, *23*, GB1005, doi:10.1029/2008GB003349.
Hausmann, U., and A. Czaja (2012), The observed signature of mesoscale eddies in sea surface temperature and the associated heat transport, *Deep Sea Res. Part I*, *70*, 60–72.
Jiang, C., S. T. Gille, J. Sprintall, and C. Sweeney (2014), Drake passage oceanic pCO_2: Evaluating CMIP5 coupled carbon-climate models using in situ observations, *J. Clim.*, *27*, 76–100.
Kahru, M., B. G. Mitchell, S. T. Gille, C. D. Hewes, and O. Holm-Hansen (2007), Eddies enhance biological production in the Weddell-Scotia Confluence of the Southern Ocean, *Geophys. Res. Lett.*, *34*, L14603, doi:10.1029/2007GL030430.
Korb, R. E., and M. Whitehouse (2004), Contrasting primary production regimes around South Georgia, Southern Ocean: Large blooms versus high nutrient, low chlorophyll waters, *Deep Sea Res., Part I*, *51*, 721–738, doi:10.1016/j.dsr.2004.02.006.
Koszalka, I., L. Ceballos, and A. Bracco (2010), Vertical mixing and coherent anticyclones in the ocean: The role of stratification, *Nonlinear Processes Geophys.*, *17*, 37–47.
Kunze, E. (1985), Near-inertial wave propagation in geostrophic shear, *J. Phys. Oceanogr.*, *15*, 544–565.
Kunze, E., R. W. Schmitt, and J. M. Toole (1995), The energy balance in a warm-core ring's near-inertial critical layer, *J. Phys. Oceanogr.*, *25*, 942–956.
Landschützer, P., N. Gruber, D. C. E. Bakker, and U. Schuster (2014), Recent variability of the global ocean carbon sink, *Global Biogeochem. Cycles*, *28*, 927–949, doi:10.1002/2014GB004853.
Landschützer, P., et al. (2015), The reinvigoration of the Southern Ocean carbon sink, *Science*, *349*(6253), 1221–1224, doi:10.1126/science.aab2620.
Large, W., J. McWilliams, and S. Doney (1994), Oceanic vertical mixing: A review and a model with nonlocal boundary layer parameterization, *Rev. Geophys.*, *32*, 363–403.
Large, W. G., and S. G. Yeager (2009), The global climatology of an interannually varying air-sea flux data set, *Clim. Dyn.*, *33*, 341–364, doi:10.1007/s00382-008-0441-3.
Lenton, A., R. J. Matear, and B. Tilbrook (2006), Design of an observational strategy for quantifying the Southern Ocean uptake of CO_2, *Global Biogeochem. Cycles*, *20*, GB4010, doi:10.1029/2005GB002620.
Lenton, A., et al. (2013), Sea-air CO_2 fluxes in the Southern Ocean for the period 1990-2009, *Biogeosciences*, *10*(6), 4037–4054, doi:10.5194/bg-10-4037-2013.

Le Quéré, C., T. Takahashi, E. T. Buitenhuis, C. Rödenbeck, and S. C. Sutherland (2010), Impact of climate change and variability on the global oceanic sink of CO_2, *Global Biogeochem. Cycles*, *24*, GB4007, doi:10.1029/2009GB003599.
Lovenduski, N. S., N. Gruber, S. C. Doney, and I. D. Lima (2007), Enhanced CO_2 outgassing in the Southern Ocean from a positive phase of the Southern Annular Mode, *Global Biogeochem. Cycles*, *21*, GB2026, doi:10.1029/2006GB002900.
Lovenduski, N. S., M. C. Long, P. R. Gent, and K. Lindsay (2013), Multi-decadal trends in the advection and mixing of natural carbon in the Southern Ocean, *Geophys. Res. Lett.*, *40*, 139–142, doi:10.1029/2012GL054483.
Luo, C., N. Mahowald, T. Bond, P. Y. Chuang, P. Artaxo, R. Siefert, Y. Chen, and J. Schauer (2008), Combustion iron distribution and deposition, *Global Biogeochem. Cycles*, *22*, GB1012, doi:10.1029/2007GB002964.
Mahadevan, A., M. Lévy, and L. Mémery (2004), Mesoscale variability of sea surface pCO2: What does it respond to?, *Global Biogeochem. Cycles*, *18*, GB1017, doi:10.1029/2003GB002102.
Majkut, J. D., J. L. Sarmiento, and K. B. Rodgers (2014), A growing oceanic carbon uptake: Results from an inversion study of surface pCO_2 data, *Global Biogeochem. Cycles*, *28*, 335–351, doi:10.1002/2013GB004585.
Marshall, J., C. Hill, L. Perelman, and A. Adcroft (1997a), Hydrostatic, quasi-hydrostatic, and nonhydrostatic ocean modeling, *J. Geophys. Res.*, *102*, 5733–5752.
Marshall, J., A. Adcroft, C. Hill, L. Perelman, and C. Heisey (1997b), A finite-volume, incompressible Navier Stokes model for studies of the ocean on parallel computers, *J. Geophys. Res.*, *102*, 5753–5766.
Marshall, J., H. Jones, and C. Hill (1998), Efficient ocean modeling using non-hydrostatic algorithms, *J. Mar. Syst.*, *18*, 115–134.
Meredith, M. P., J. L. Watkins, E. J. Murphy, N. J. Cunningham, A. G. Wood, R. Korb, M. J. Whitehouse, S. E. Thorpe, and F. Vivier (2003), An anticyclonic circulation above the Northwest Georgia Rise, Southern Ocean, *Geophys. Res. Lett.*, *30*(20), 2061, doi:10.1029/2003GL018039.
Merlivat, L., J. Boutin, and D. Antoine (2015), Roles of biological and physical processes in driving seasonal air–sea CO_2 flux in the Southern Ocean: New insights from CARIOCA pCO_2, *J. Mar. Syst.*, *147*, 9–20.
Metzl, N. (2009), Decadal increase of oceanic carbon dioxide in Southern Indian Ocean surface waters (1991–2007), *Deep Sea Res., Part II*, *56*, 607–619, doi:10.1016/j.dsr2.2008.12.007.
Metzl, N., C. Brunet, A. Jabaud-Jan, A. Poisson, and B. Schauer (2006), Summer and winter air-sea CO_2 fluxes in the Southern Ocean, *Deep Sea Res., Part I*, *53*, 1548–1563, doi:10.1016/j.dsr.2006.07.006.
Mikaloff Fletcher, S. E., et al. (2006), Inverse estimates of anthropogenic CO_2 uptake, transport, and storage by the ocean, *Global Biogeochem. Cycles*, *20*, GB2002, doi:10.1029/2005GB002530.
Munro, D. R., N. S. Lovenduski, T. Takahashi, B. B. Stephens, T. Newberger, and C. Sweeney (2015a), Recent evidence for a strengthening CO2 sink in the Southern Ocean from carbonate system measurements in the Drake Passage (2002–2015), *Geophys. Res. Lett.*, *42*, 7623–7630, doi:10.1002/2015GL065194.
Munro, D. R., et al. (2015b), Estimates of net community production in the Southern Ocean determined from time series observations (2002-2011) of nutrients, dissolved inorganic carbon, and surface ocean pco_2 in Drake Passage, *Deep Sea Res., Part II*, *114*, 49 – 63, doi:10.1016/j.dsr2.2014.12.014.
Paparazzo, F. E., L. Bianucci, I. R. Schloss, G. O. Almandoz, M. Solís, and J. L. Esteves (2010), Cross-frontal distribution of inorganic nutrients and chlorophyll-a on the Patagonian Continental Shelf of Argentina during summer and fall, *Rev. Biol. Mar. Oceanogr.*, *45*(1), 107–119.
Parekh, P., M. J. Follows, S. Dutkiewicz, and T. Ito (2006), Physical and biological regulation of the soft tissue carbon pump, *Paleoceanography*, *21*, PA3001, doi:10.1029/2005PA001258.
Sarmiento, J. L., and N. Gruber (2006), *Ocean Biogeochemical Dynamics*, 503 pp., Princeton Univ. Press, Princeton, N. J.
Song, H., J. Marshall, P. Gaube, and D. J. McGillicuddy (2015), Anomalous chlorofluorocarbon uptake by mesoscale eddies in the Drake Passage region, *J. Geophys. Res. Oceans*, *120*, 1065–1078, doi:10.1002/2014JC010292.
Song, H., J. Marshall, M. J. Follows, S. Dutkiewicz, and G. Forget (2016), Source waters for the highly productive Patagonian shelf in the southwestern Atlantic, *J. Mar. Syst.*, *158*, 120–128.
Sprintall, J., T. K. Chereskin, and C. Sweeney (2012), High-resolution underway upper ocean and surface atmospheric observations in drake passage: Synergistic measurements for climate science, *Oceanography*, *25*(3), 70–81, doi:10.5670/oceanog.2012.77.
Stephenson, G. R. J., S. T. Gille, and J. Sprintall (2013), Processes controlling upper-ocean heat content in Drake Passage, *J. Geophys. Res. Oceans*, *118*, 4409–4423, doi:10.1002/jgrc.20315.
Tagliabue, A., J.-B. Sallée, A. R. Bowie, M. Lévy, S. Swart, and P. W. Boyd (2014), Surface-water iron supplies in the Southern Ocean sustained by deep winter mixing, *Nat. Geosci.*, *7*, 314–320, doi:10.1038/ngeo2101.
Takahashi, T., J. Olafsson, J. G. Goddard, D. W. Chipman, and S. C. Sutherland (1993), Seasonal variation of CO_2 and nutrients in the high-latitude surface oceans: A comparative study, *Global Biogeochem. Cycles*, *7*, 843–878.
Takahashi, T., et al. (2002), Global sea-air CO_2 flux based on climatological surface ocean pCO_2, and seasonal biological and temperature effects, *Deep Sea Res., Part II*, *49*, 1601–1622.
Takahashi, T., S. Sutherland, D. Chipman, J. Goddard, C. Ho, T. Newberger, C. Sweeney, and D. Munro (2014a), Climatological distributions of pH, pCO_2, total CO_2, alkalinity, and $CaCO_3$ saturation in the global surface ocean, and temporal changes at selected locations, *Mar. Chem.*, *164*, 95–125, doi:10.1016/j.marchem.2014.06.004.
Takahashi, T., S. C. Sutherland, D. W. Chipman, J. G. Goddard, T. Newberger, and C. Sweeney (2014b), Climatological Distributions of pH, pCO_2, Total CO_2, Alkalinity, and $CaCO_3$ Saturation in the Global Surface Ocean, *Tech. Rep. ORNL/CDIAC-160, NDP-094*, Carbon Dioxide Inf. Anal. Cent., Oak Ridge Natl. Lab., U.S. Dep. of Energy, Oak Ridge, Tenn., doi:10.3334/CDIAC/OTG.NDP094.
Thomalla, S. J., N. Fauchereau, S. Swart, and P. M. S. Monteiro (2011), Regional scale characteristics of the seasonal cycle of chlorophyll in the Southern Ocean, *Biogeosciences*, *8*, 2849–2866.
Tulloch, R., et al. (2014), Direct estimates of lateral eddy diffusivity upstream of Drake Passage, *J. Phys. Oceanogr.*, *44*, 2593–2616.
Verdy, A., S. Dutkiewicz, M. J. Follows, J. Marshall, and A. Czaja (2007), Carbon dioxide and oxygen fluxes in the Southern Ocean: Mechanisms of interannual variability, *Global Biogeochem. Cycles*, *21*, GB2020, doi:10.1029/2006GB002916.
Wanninkhof, R. (1992), Relationship between wind speed and gas exchange over the ocean, *J. Geophys. Res.*, *97*, 7373–7382, doi:10.1029/92JC00188.
Watson, A. J., D. C. E. Bakker, A. J. Ridgwell, P. W. Boyd, and C. S. Law (2000), Effect of iron supply on Southern Ocean CO_2 uptake and implications for glacial atmospheric CO_2, *Nature*, *407*(6805), 730–733.
Williams, R. G. (1988), Modification of ocean eddies by air-sea interaction, *J. Geophys. Res.*, *93*, 15,523–15,533.
Xue, L., L. Gao, W.-J. Cai, W. Yu, and M. Wei (2015), Response of sea surface fugacity of CO_2 to the SAM shift south of Tasmania: Regional differences, *Geophys. Res. Lett.*, *42*, 3973–3979, doi:10.1002/2015GL063926.